

# Carbon-coated titania nanostructured particles: Continuous, one-step flame-synthesis

Hendrik K. Kammler and Sotiris E. Pratsinis<sup>a)</sup>

Particle Technology Laboratory Department of Mechanical and Process Engineering,  
ETH Zurich, Sonneggstrasse 3, ML F25, CH-8092 Zurich, Switzerland

(Received 26 May 2003; accepted 14 August 2003)

Concurrent synthesis of titania-carbon nanoparticles (up to 52 wt.% in C) was studied in a diffusion flame aerosol reactor by combustion of titanium tetraisopropoxide and acetylene. These graphitically layered carbon-coated titania particles were characterized by high-resolution transmission electron microscopy (HRTEM), with elemental mapping of C and Ti, x-ray diffraction (XRD), and nitrogen adsorption [Brunauer–Emmett–Teller (BET)]. The specific surface area of the powder was controlled by the acetylene flow rate from 29 to 62 m<sup>2</sup>/g as the rutile content decreased from 68 to 17 wt.%. Light blue titania suboxides formed at low acetylene flow rates. The average XRD crystal size of TiO<sub>2</sub> decreased steadily with increasing carbon content of the composite powders, while the average BET primary particle size calculated from nitrogen adsorption decreased first and then approached a constant value. The latter is attributed to the formation of individual carbon particles next to carbon-coated titania particles as observed by HRTEM and electron spectroscopic imaging.

## I. INTRODUCTION

Carbon coatings on ceramic particles can improve their dispersibility in polymers, drastically increase the electrical conductivity of ceramic composites,<sup>1</sup> and carbon-coated particles could be used as gray pigments. Furthermore, carbon-coated metal oxides are important for fillers in rubber for the so-called “green tires” and as precursors to synthesis of the corresponding carbides. Typically, these products are made by separate synthesis of the oxide and carbon particles followed by cumbersome powder mixing. Flame technology can offer an alternative synthesis route for these products with closely controlled composition without the multiple steps and high liquid volumes associated with wet chemical processes or long processing times associated with solid processing of materials.<sup>2</sup>

Carbon-coated silica was made in acetylene/SiCl<sub>4</sub> premixed flames by Spicer *et al.*,<sup>3</sup> who found a significant increase in the carbon yield (up to three times) in the presence of silica compared with a pure acetylene flame of the same equivalence ratio. This was attributed to the presence of silica particles acting as seed nuclei for carbon surface growth, as well as to the chlorine presence reducing the flame temperature. Silica-carbon particles with carbon contents up to 5 wt.% were synthesized in a ring-shaped double diffusion hexamethyl

disiloxane (HMDSO)-oxygen flame at production rates up to 130 g/h by Kammler *et al.*,<sup>4</sup> and recently the pilot-scale production (up to 700 g/h) of silica-carbon nanostructured particles in a hydrogen-air diffusion flame was demonstrated.<sup>5</sup>

Carbon-coated titania has been used by Koc and co-workers<sup>6–9</sup> as a precursor for TiC powder production. Thereby, they coated commercially available TiO<sub>2</sub> powders with carbon by decomposing C<sub>3</sub>H<sub>6</sub> at 300–600 °C batch wise using multiple coating cycles (e.g., 18 cycles lasting 20 min each to obtain 32.6 wt.% carbon<sup>7</sup>). These powders were then transformed to TiC at 1200–1550 °C. Another process for coating metal oxide powders with carbon was introduced recently by Inagaki and co-workers,<sup>10,11</sup> heating oxide powders (30–200 μm) together with polyvinylchloride for 1 h at about 1000 °C. They attributed the observed suppression of anatase to rutile phase transformation to the carbon layer that could prevent crystal growth and sintering. Furthermore, they proposed that the carbon layer also enhanced the adsorption of methylene blue during ultraviolet (UV) irradiation experiments and that it prevented interaction between TiO<sub>2</sub> and binder polymer, which decomposes the polymer under UV irradiation.

The goal of this study was to explore the potential of continuous flame aerosol reactors for synthesis of carbon-coated titania of controlled composition in a single-step process using flame technology that has an established potential for process scale-up.<sup>5</sup> More specifically, these particles were made by combustion of

<sup>a)</sup>Address all correspondence to this author.  
e-mail: [pratsinis@ptl.mavt.ethz.ch](mailto:pratsinis@ptl.mavt.ethz.ch)

acetylene and titanium tetrakisopropoxide (TTIP) in a flame reactor, and the effect of the fuel/precursor flow rate on the product powder characteristics was investigated by microscopy, x-ray diffraction (XRD), and nitrogen adsorption.

## II. EXPERIMENTAL

A schematic of the experimental setup is shown in Fig. 1. Powders are produced in a stainless steel conical diffusion flame reactor, consisting of three concentric tubes. The inner diameter of the central tube is 4.8 mm, while the subsequent first and second annuli have inner–outer diameters of 5.6–6.4 mm and 7.3–9 mm, respectively. A mixture of TTIP/nitrogen (99.9995% Pangas, Zurich, Switzerland) and 0.2–0.65 l/min acetylene (99.99% Pangas) is fed through the central tube. In the first annulus, 0.05 l/min nitrogen is provided to prevent particle deposition on the burner mouth,<sup>12</sup> and 1.15 l/min air is fed through the second annulus. An evaporator system [Bronkhorst CEM 100W (evaporator), Bronkhorst EL-Flow201 (gas mass flow controller), and Bronkhorst Liqui-Flow L1 (liquid mass flow controller)]<sup>13</sup> delivers titanium tetrakisopropoxide (TTIP, Aldrich, >97%, distilled over vacuum prior to use) at 145 °C into the burner, using 1.13 l/min nitrogen as carrier gas resulting in 5 g/h TiO<sub>2</sub>. The reactant composition in the flame is characterized by the equivalence ratio (EQR), which is the fuel (acetylene and TTIP) to oxidant molar ratio to the stoichiometric fuel to oxidant ratio.<sup>14</sup>

The product powder (5–8 g/h, depending on the carbon content) is collected on glass fiber filters (Whatman GF/A, 15 cm in diameter) using a vacuum pump (Vacuubrand RE8, Germany). The Brunauer–Emmett–Teller

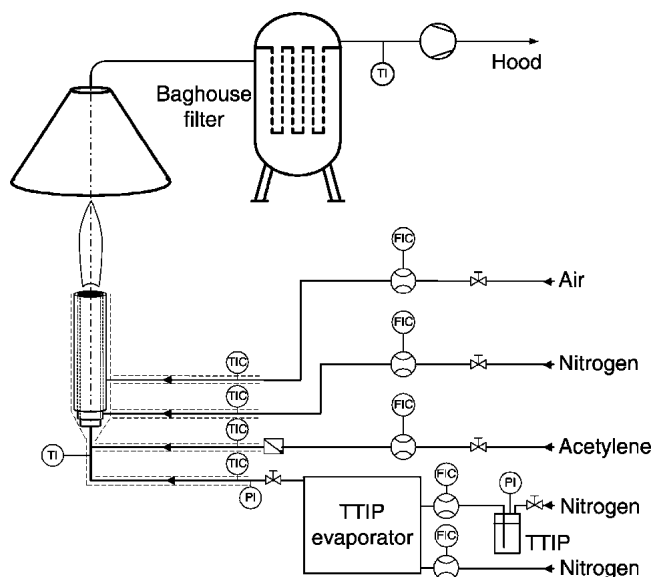


FIG. 1. Experimental set-up for single-step, continuous production of carbon-coated titania nanoparticles in a diffusion flame reactor.

(BET)-equivalent specific surface area (SSA) of the product powder is determined from a 5 point nitrogen adsorption isotherm in the relative pressure range  $p/p_0 = 0.05$  to 0.25 (Tristar, Micromeritics Instruments Corp.). The average primary particle diameter is calculated by  $d_{\text{BET}} = 6 / (\rho \times \text{SSA})$ , where  $\rho$  is the particle density. The rutile content and crystal size<sup>15</sup> are obtained by XRD (Bruker D8 advance diffractometer, 40 kV, 40 mA, Bragg–Brentano geometry,  $2\theta = 20^\circ$  to  $70^\circ$ , step size  $0.02^\circ$ , at a scan speed of  $0.24^\circ/\text{min}$ ) using the fundamental parameter approach (Rietveld method).<sup>15</sup> The carbon content is determined by thermogravimetric analysis (TGA) with a thermobalance (TGA/SDTA851<sup>e</sup>, LF/1100 °C, Mettler-Toledo AG) using a standard heating sequence.<sup>5</sup>

The transmission electron microscope (TEM) pictures of the product powder were taken with a Zeiss electron microscope 912 Omega with ProScan and slow scan charge-coupled device (CCD) camera operated at 100 kV, while the high-resolution (HR) TEM images were obtained with a CM30ST microscope (Philips, LaB6 cathode, operated at 300 kV). Furthermore, TEM for the electron energy loss spectra (EELS) were performed with a Tecnai F30 FEG microscope (Philips, Schottky field emitter, operated at 300 kV). The TEM images were recorded close to Scherzer defocus or at an even higher defocus to increase the image contrast. An energy filter [Gatan imaging filter, (GIF)], which is installed below the Tecnai F30 FEG, allows recording EELS and element specific images (elemental maps) by means of the electron spectroscopic imaging (ESI) technique. The so-called three-window method was applied for the mappings: An image is taken after a suitable ionization edge of the corresponding element (post-edge image,  $\Delta E_3$ ), two additional images (pre-edge 1,  $\Delta E_1$ , and pre-edge 2,  $\Delta E_2$ ) are recorded at energy losses smaller than the ionization edge. Only the electrons passing through a selected energy slit (8–30 eV wide) contribute to these images. Specimen drift during recording of these images is compensated for by a cross-correlation algorithm implemented in the software of the GIF (Digital Micrograph, Gatan). The pre-edge images are used for an approximate determination of the unspecific background, which is then subtracted from the post-edge image leading to an elemental map with enhanced contrast. The image series were recorded with a Slow Scan CCD camera (2048 × 2048 pixels), and ESI images were calculated with the software Digital Micrograph.

## III. RESULTS

Figure 2 shows XRD patterns of the carbon-titania powders made at 0.2, 0.3, 0.46, and 0.65 l/min acetylene flow rate resulting in 0.5, 15, 40, and 52 wt.% C, respectively. At the investigated process conditions

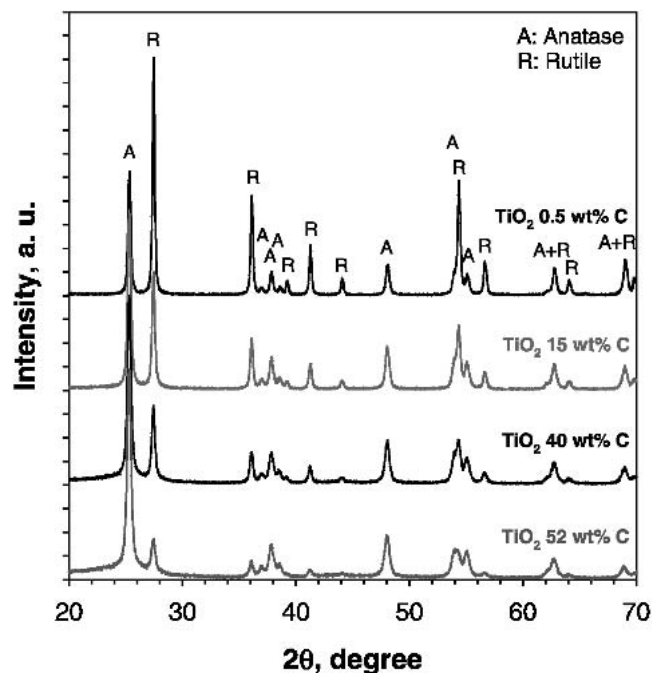


FIG. 2. X-ray diffraction pattern of flame-made carbon-coated TiO<sub>2</sub> with 0.5, 15, 40, and 52 wt.% C prepared in this work. A and R indicate the anatase and rutile peaks, respectively.

(0.5–52 wt.% C) no TiC was formed during simultaneous formation of carbon and TiO<sub>2</sub>. Increasing the carbon content decreases the rutile content of the powders, consistent with the results of Inagaki and co-workers.<sup>10,11</sup> The thermogravimetric analysis (TGA) curves (not shown) of the carbon-titania powders showed a slight decrease of 0.5–1 wt.% when heating up the powders from 120 to 800 °C under nitrogen atmosphere followed by a rapid weight loss (0.5–52 wt.%, depending on the C-content) when switching the atmosphere to oxygen at 800 °C. The former weight loss can be attributed to removal of chemisorbed water, surface OH-groups and any volatile organic compounds, while the latter is directly related to non-volatile carbon (soot) oxidation and removal as CO<sub>2</sub> or CO.<sup>5,16</sup> The sample weight remains constant when further heating the powder to 1000 °C, since the TiO<sub>2</sub> surface is free of OH groups at this temperature.<sup>16</sup>

Figure 3 shows TEM pictures of the carbon-titania powders containing (a) 15 wt.% and (b) 52 wt.% carbon, respectively, as well as HRTEM of the corresponding powders (c) 15 wt.% and (d) 52 wt.%. The degree of agglomeration of these particles is similar to commercially available, similarly sized TiO<sub>2</sub> (Degussa P25). Coated TiO<sub>2</sub> particles can be observed clearly in Figs. 3(a) and 3(b). In the HRTEMs [Figs. 3(c) and 3(d)] the typical curved shape of the graphitic layer structure of carbon can be clearly distinguished from the linear TiO<sub>2</sub> lattice structure. The thickness of this C coating layer is 2–3 nm, relatively homogeneous through all particles and

does not seem to depend on the carbon content from 15–52 wt.% carbon. At 52 wt.% carbon, some noncoated particles can be observed [lower right part in Fig. 3(b) and lower left part in Fig. 3(d)]. Elemental mappings of C and Ti are shown in Fig. 4 for the samples of Fig. 3. These pictures further corroborate that the carbon is relatively homogeneously distributed on the TiO<sub>2</sub> surface. In addition, at higher carbon content (e.g., 52 wt.%) pure carbon particles are formed next to the carbon-coated TiO<sub>2</sub> [Figs. 4(e) and 4(f)]. In the 15 wt.% carbon-TiO<sub>2</sub> fewer pure carbon particles were detected (not shown). Furthermore, in all powders, sparsely, a few uncoated TiO<sub>2</sub> particles were detected during extensive HRTEM and elemental mapping analysis.

Figure 5 shows the specific surface area (SSA, circles, left axis) and the rutile content (triangles, right axis) of the carbon-titania powders as a function of the acetylene flow rate. Increasing the acetylene flow rate from 0.2 to 0.65 l/min increases the SSA from 29 to 62 m<sup>2</sup>/g. The SSA increases rapidly from 0.2 to 0.3 l/min of acetylene and then slower reaching nearly an asymptotic value (~60 m<sup>2</sup>/g) at higher the acetylene flow rates (>0.5 l/min). The XRD rutile content decreases sharply from 68 to 40 wt.% by increasing the acetylene flow rate from 0.2 to 0.3 l/min, and then decreases to 17 wt.% when the acetylene flow rate is further increased to 0.65 l/min.

Figure 6 shows the carbon content of the powders of Fig. 5 as a function of the acetylene flow rate. Up to 0.2 l/min acetylene flow, hardly any carbon (0.5 wt.%) is detected in the product powder that appears light blue indicating titania suboxides. With increasing acetylene flow rate to 0.65 l/min the carbon content of the powder increases steadily up to 52 wt.%. The visual appearance of the powders changes from light blue (0.2 l/min C<sub>2</sub>H<sub>2</sub>) to dark blue up to 0.32 l/min C<sub>2</sub>H<sub>2</sub> to black for more than 0.32 l/min C<sub>2</sub>H<sub>2</sub> (Fig. 6).

When the weighed particle diameter from nitrogen adsorption is calculated using  $\rho_{\text{anatase}} = 3.84 \text{ g/cm}^3$ ,  $\rho_{\text{rutile}} = 4.26 \text{ g/cm}^3$ , and  $\rho_{\text{carbon}} = 1.8 \text{ g/cm}^3$  for soot<sup>17</sup> (or 2.27 g/cm<sup>3</sup> for graphite<sup>18</sup>) as well as the average XRD crystallite size<sup>15</sup> (Fig. 2) as functions of the powder carbon content, two distinct regimes are observed (Fig. 7). If the carbon content increases from 0.5 to 15 wt.%, the  $d_{\text{XRD}}$  (circles) and the  $d_{\text{BET}}$  decrease sharply (from 58 to 39 nm and from 52 to 37 nm, respectively). The  $d_{\text{XRD}}$  decreases less pronounced from 39 to 24 nm, when further increasing the carbon content from 15 to 52 wt.%, while the  $d_{\text{BET}}$  stays almost constant at about 38 nm (using the soot density, squares) or at 34 nm (using the graphite density, triangles). These primary particle sizes ( $d_{\text{BET}}$  and  $d_{\text{XRD}}$ ) agree well with the corresponding sizes observed by TEM (Fig. 3) indicating single crystals. The carbon-yield [carbon detected in the product powder divided by the carbon (acetylene and TTIP)

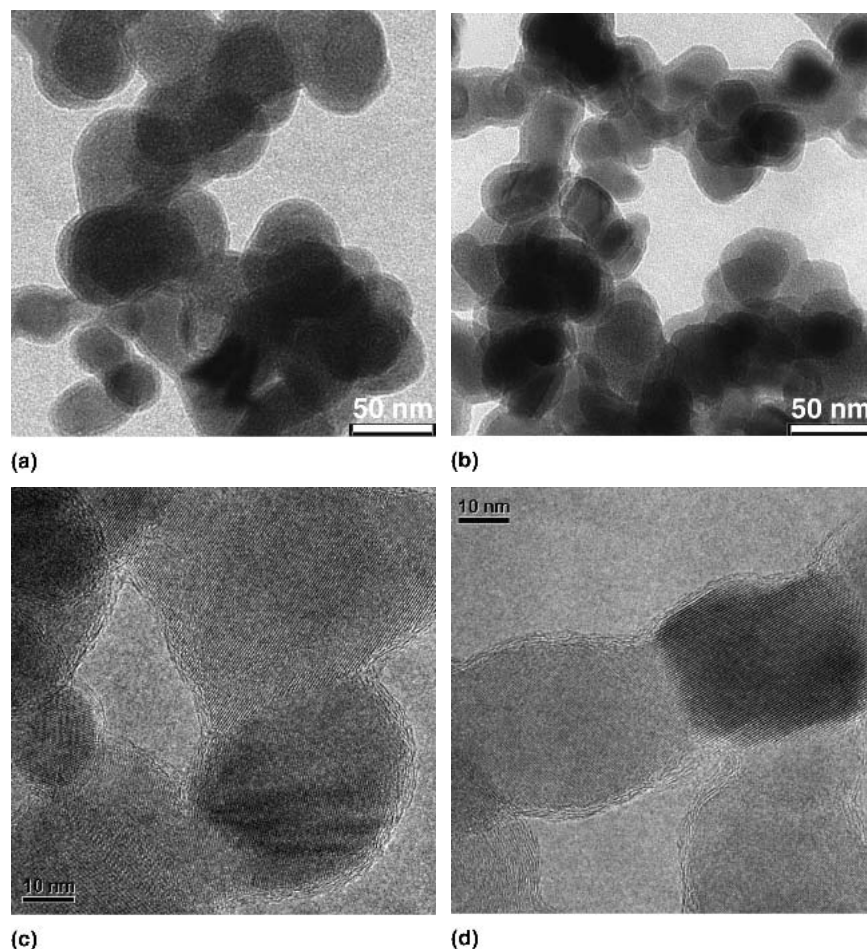


FIG. 3. Transmission electron micrographs of flame-made carbon-coated titania with (a) 15 wt.% and (b) 52 wt.% carbon and HRTEMs of the same powders (c) 15 wt.% and (d) 52 wt.%. The particles in the lower right part of (b) and lower left part of (d) are not coated and do not contain crystal reflections that are typical for crystalline  $\text{TiO}_2$  suggesting that these are carbon particles coexisting with carbon-coated titania particles that can be observed in the other parts of this picture.

fed to the system] is in the order of 5% for the highest acetylene flow rates ( $>0.37$  l/min), which is in agreement to that observed for carbon-coating of fumed silica.<sup>3</sup> The rest of the carbon was used in the combustion process.

#### IV. DISCUSSION

Increasing the acetylene flow rate from 0.2 to 0.65 l/min increases the excess of fuel in the flame significantly (EQR increases from 4.2 to 8.8). Since the combustion temperature is lowered by increasing the EQR,<sup>19</sup> the SSA increases as observed in Fig. 5. This is in agreement with flame aerosol synthesis of carbon-silica powder.<sup>3</sup> At these fuel-rich conditions, lower EQRs (EQR = 4.2 at 0.2 l/min  $\text{C}_2\text{H}_2$ ) result in higher temperatures that increase carbon oxidation (Fig. 6) and the sintering rate of titania particles. This is consistent with the high rutile content of powders at high temperatures<sup>20</sup> made at low acetylene flow rates (Fig. 5).

After the  $\text{TiO}_2$  is coated with carbon, adding more carbon (up to 15 wt.% carbon) first leads to a less sparse and thicker layer as observed by TEM while the  $\text{TiO}_2$  particle size decreases with increasing acetylene flow rate (Fig. 7). At even higher carbon contents ( $>10$  wt.%), the  $d_{\text{XRD}}$  decreases rather slowly with increasing carbon content (Fig. 7), since carbon appears to hinder  $\text{TiO}_2$  sintering and through the reduced flame temperature that decreases the sintering rate.<sup>11</sup> The particle diameter calculated from nitrogen adsorption data (specific surface area), however, stays constant. HRTEM pictures show a carbon layer of 2–3 nm covering the  $\text{TiO}_2$  particles (Figs. 3 and 4). Calculating the amount of carbon that is needed to cover primary particles of  $d_{\text{XRD}} = 39$  nm [Figs. 3(a), 3(c), and 4(a)–4(c)] with a 2.3-nm-thick C layer (using  $\rho_{\text{C}} = 1.8^{17}$ ) or 1.9-nm-thick C layer (using  $\rho_{\text{C}} = 2.27^{18}$ ) results in powders containing 15 wt.% carbon. This is in good agreement with thickness of the C layer observed from TEM for the 15 wt.% C and consistent with the EELS measurements,

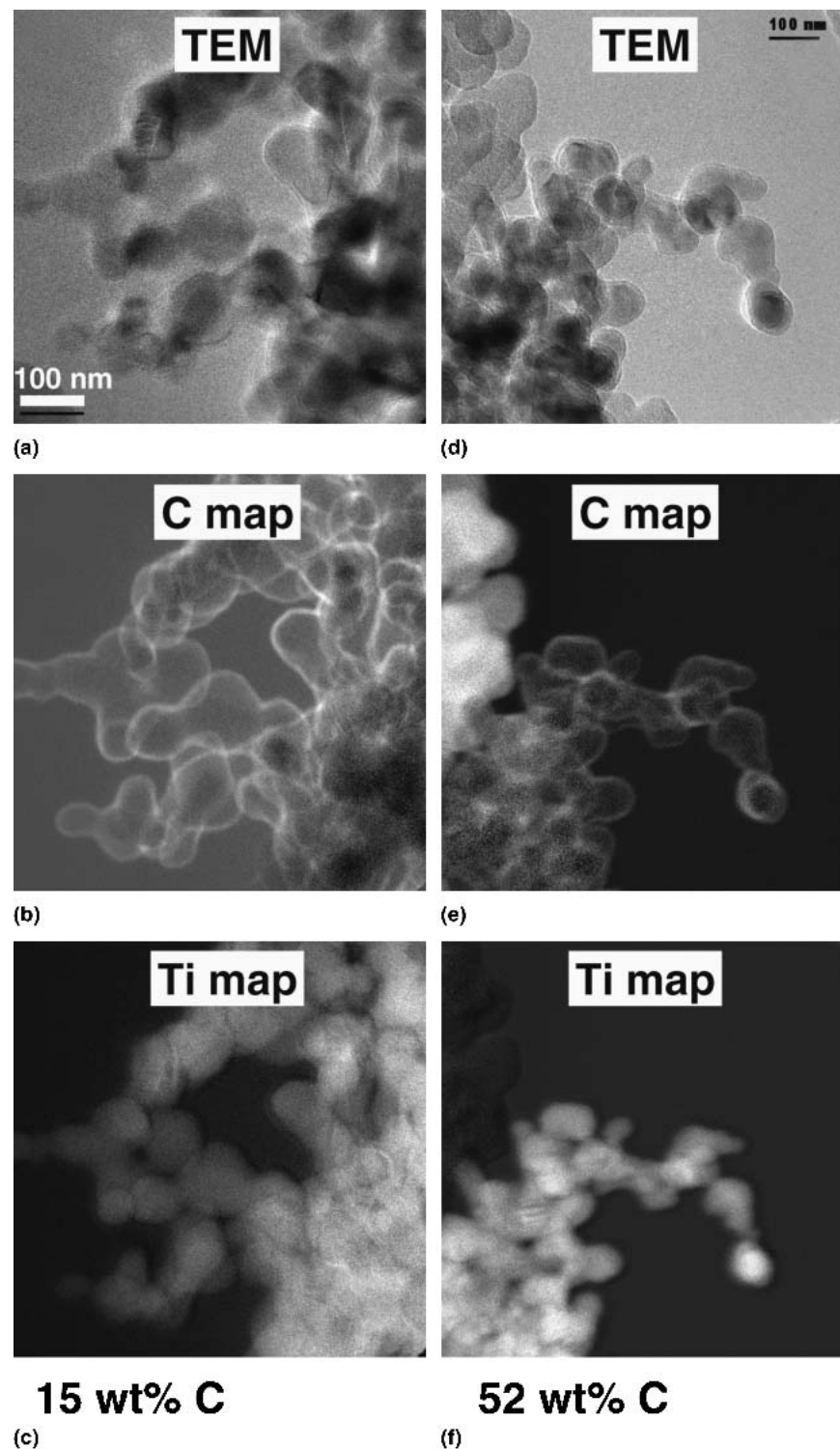


FIG. 4. (a,d) Transmission electron micrographs along with the corresponding (b,e) elemental C and (c,f) Ti maps for carbon-TiO<sub>2</sub> powders containing (a–c) 15 wt.% and (d–f) 52 wt.% C.

where carbon coated TiO<sub>2</sub> and almost no separate carbon particles were detected. Thus, the produced carbon is bound almost completely to the TiO<sub>2</sub> surface at these process conditions.

From TEM (Fig. 3) it becomes apparent that the 2–3-nm carbon layer does not increase in thickness with increasing the carbon content of the powder from 15 wt.% [Fig. 3(c)] to 52 wt.% [Fig. 3(d)] as one might have

expected from the evolution of the specific surface area (Fig. 5). Here, pure carbon particles are formed next to carbon-coated titania as can be observed in the lower right part of Fig. 3(b) and the lower left part of Fig. 3(d), for example. These particles are not coated and do not contain the crystal reflections typical for  $\text{TiO}_2$ . Therefore, these particles should be pure carbon particles that

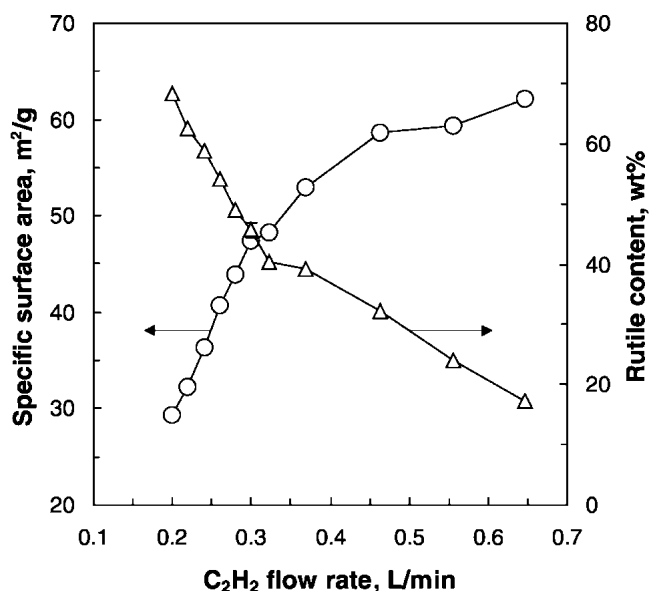


FIG. 5. Specific surface area (circles) and rutile content (triangles) of carbon-titania nanostructured powders as a function of acetylene flow rate fed to the diffusion flame aerosol reactor.

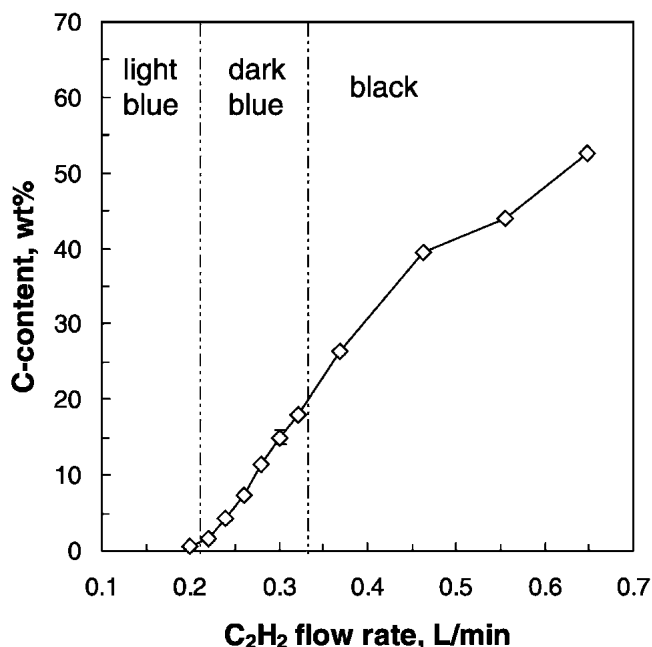


FIG. 6. Carbon content and regions of visual powder appearance of carbon-titania nanostructured powders as a function of the acetylene flow rate fed to the diffusion flame aerosol reactor.

coexist with the carbon-coated titania as was confirmed by elemental mapping of C and Ti (Fig. 4). These pure carbon particles grow even to larger sizes when increasing the acetylene flow rate or the overall carbon content of the powder that decreases the specific surface area (Fig. 5). However, the average primary particle diameter remains almost constant with increasing acetylene flow rate (0.3–0.65 l/min) as the overall density of the mixed carbon-titania powder decreases (Fig. 7). The amount of carbon that is needed for covering 27-nm-diameter  $\text{TiO}_2$  particles (which corresponds to  $d_{\text{XRD}}$  of the  $\text{TiO}_2$  powder containing 52 wt.% C) completely with a 2- or 3-nm carbon-layer, is 19 or 28 wt.% C (using  $\rho_{\text{C}} = 1.8^{17}$ ) and 23 or 32 wt.% C (using  $\rho_{\text{C}} = 2.27^{18}$ ). Since in the present case 52 wt.% C powders were produced, this indicates that about half of the carbon is used for the  $\text{TiO}_2$  coating while the rest forms individual (pure) carbon particles consistent with TEM [Figs. 3(b), 3(d), and 4(d)–4(f)].

These flame-made carbon-coated  $\text{TiO}_2$  powders differ from those made by Koc and co-workers<sup>6</sup> that contained porous carbon layers covering the  $\text{TiO}_2$  particles, since adsorption/desorption isotherms of the present flame-made powders revealed them to be non-porous. These isotherms exhibited only a slight hysteresis at high relative pressures, which was even less pronounced than that shown by Stark *et al.*<sup>21</sup> for flame-made vanadia-doped titania. This hysteresis is attributed to the sintering necks

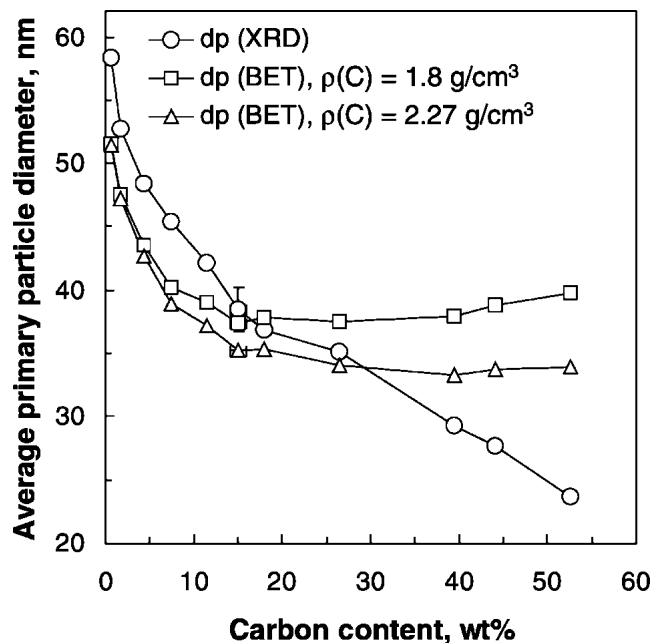


FIG. 7. Average crystal size (circles) of titania (obtained by XRD) and average primary particle size (obtained by nitrogen adsorption, BET) of the nanostructured carbon-titania powders as a function of their carbon content. Here, two densities for carbon [soot<sup>17</sup> (squares) and graphite<sup>18</sup> (triangles)] were used to calculate the average BET particle diameter.

between the agglomerated primary particles. The present process has the advantage that the used precursors for TiO<sub>2</sub> and carbon (TTIP and acetylene) do not contain halide compounds as that in the process of Inagaki *et al.*<sup>10</sup> Furthermore, the formation of sub-stoichiometric titania might be advantageous during further processing of this powder to TiC, since Swift and Koc<sup>8</sup> showed that the formation of TiC from carbon-coated TiO<sub>2</sub> proceeds through the formation of lower oxides of titania (TiO<sub>2-x</sub>). The flame-made particles are of high purity (TGA results),<sup>5,16</sup> and they are typically of a narrow size distribution with geometric standard distributions between 1.4 and 1.8.<sup>22</sup> If for certain applications even the present low degree of agglomeration of the TiO<sub>2</sub> (single particles, doublets and triplets) is too high, the process conditions can easily be adjusted to produce non-agglomerated TiO<sub>2</sub> as demonstrated recently.<sup>22</sup>

## V. CONCLUSIONS

The feasibility of a continuous, one-step process for synthesis of carbon-coated titania particles with closely controlled characteristics was presented. Homogeneously coated particles were produced in a diffusion flame aerosol reactor with carbon contents from 0.5 to 52 wt.% and a graphitic carbon layer thickness of up to 3 nm at production rates up to 8 g/h. For powders containing up to 15 wt.% carbon, nearly all carbon is bound to the TiO<sub>2</sub> particles, while increasing the carbon content of the powder by increasing the acetylene flow rate resulted in the formation of separate carbon particles next to the carbon-coated titania particles but did not increase the thickness of the carbon layer of the latter ones. For TiO<sub>2</sub> powders made with the highest carbon content (52 wt.% C) roughly half of the carbon is used for coating, while the rest forms individual (pure) carbon particles in agreement with TEM. The specific surface area and crystallinity of the carbon titania powder was closely controlled by the acetylene flow rate. Doubling the acetylene flow rate increased the specific surface area from 29 to 62 m<sup>2</sup>/g, while at the same time the rutile content of the powders decreased drastically from 68 to 17 wt.%. Furthermore, the color of the product powder changed from

light blue for TiO<sub>2</sub> suboxides made at low acetylene flow rates to dark blue and eventually black powders that were made at the highest carbon contents.

## ACKNOWLEDGMENTS

We acknowledge the financial support of the Swiss Commission for Technology and Innovation, KTI Top-Nano21 (287-044-01), Dr. Frank Krumeich (ETHZ) for the HRTEM and elemental mapping experiments, and Dr. Martin Müller (ETHZ) for the TEM.

## REFERENCES

1. Y. Hareyama, Patent EP 985,638 A1 (1999).
2. S.E. Pratsinis, *Prog. Energy Combust. Sci.* **24**, 197 (1998).
3. P.T. Spicer, C. Artelt, S. Sanders, and S.E. Pratsinis, *J. Aerosol Sci.* **29**, 647 (1998).
4. H.K. Kammler and S.E. Pratsinis, *J. Nanoparticle Res.* **1**, 467 (1999).
5. H.K. Kammler, R. Mueller, O. Senn, and S.E. Pratsinis, *AIChE J.* **47**, 1533 (2001).
6. R. Koc and G.C. Glatzmaier, U.S. Patent No. 5 417 952 (1995).
7. R. Koc, *J. Eur. Ceram. Soc.* **17**, 1309 (1997).
8. G.A. Swift and R. Koc, *J. Mater. Sci.* **34**, 3083 (1999).
9. R. Koc, C. Meng, and G.A. Swift, *J. Mater. Sci.* **35**, 3131 (2000).
10. M. Inagaki, H. Miura, and H. Konno, *J. Eur. Ceram. Soc.* **18**, 1011 (1998).
11. T. Tsumura, N. Kojitani, I. Izumi, N. Iwashita, M. Toyoda, and M. Inagaki, *J. Mater. Chem.* **12**, 1391 (2002).
12. H.K. Kammler and S.E. Pratsinis, *Chem. Eng. Process.* **39**, 219 (2000).
13. W.J. Stark, S.E. Pratsinis, and A. Baiker, *J. Catal.* **203**, 516 (2001).
14. S.R. Turns, *An Introduction to Combustion: Concepts and Applications*, 2nd ed. (McGraw-Hill, New York, 1996).
15. R.W. Cheary and A. Coelho, *J. Appl. Crystallogr.* **25**, 109 (1992).
16. R. Mueller, H.K. Kammler, K. Wegner, and S.E. Pratsinis, *Langmuir* **19**, 160 (2003).
17. D.F. Kronholm and J.B. Howard, Twenty-eighth Symposium (International) on Combustion (The Combustion Institute, Pittsburgh, PA, 2000), p. 2555.
18. P.W. Atkins, *Physikalische Chemie*, 2nd ed. (VCH-Verlag, Weinheim, Germany, 1990).
19. I. Glassman, *Combustion*, 3rd ed. (Academic Press, San Diego, CA, 1996).
20. K.J.D. MacKenzie, *Trans. J. Brit. Ceram. Soc.* **74**, 121 (1975).
21. W.J. Stark, K. Wegner, S.E. Pratsinis, and A. Baiker, *J. Catal.* **197**, 182 (2001).
22. H.K. Kammler, R. Jossen, P.W. Morrison, Jr., S.E. Pratsinis, and G. Beaucage, *Powder Technol.* (2003, in press).